
Hierarchical VAEs Know What They Don't Know

Jakob D. Havtorn^{1,2} Jes Frelsen¹ Søren Hauberg¹ Lars Maaløe^{1,2}

Abstract

Deep generative models have shown themselves to be state-of-the-art density estimators. Yet, recent work has found that they often assign a higher likelihood to data from outside the training distribution. This seemingly paradoxical behavior has caused concerns over the quality of the attained density estimates. In the context of hierarchical variational autoencoders, we provide evidence to explain this behavior by out-of-distribution data having in-distribution low-level features. We argue that this is both expected and desirable behavior. With this insight in hand, we develop a fast, scalable and fully unsupervised likelihood-ratio score for OOD detection that requires data to be in-distribution across all feature-levels. We benchmark the method on a vast set of data and model combinations and achieve state-of-the-art results on out-of-distribution detection.

1. Introduction

The reliability and safety of machine learning systems applied in the real-world is contingent on the ability to detect when an input is different from the training distribution. Supervised classifiers built as deep neural networks are well-known to misclassify such *out-of-distribution* (OOD) inputs to known classes with high confidence (Goodfellow et al., 2015; Nguyen et al., 2015). Several approaches have been suggested to equip deep classifiers with OOD detection capabilities (Hendrycks & Gimpel, 2017; Lakshminarayanan et al., 2017; Hendrycks et al., 2019; DeVries & Taylor, 2018). But, such methods are inherently supervised and require in-distribution labels or examples of OOD data limiting their applicability and generality.

Unsupervised generative models that estimate an explicit likelihood should understand what it means to be in- and out-of-distribution without requiring labels or examples of

¹Department of Applied Mathematics and Computer Science, Technical University of Denmark, Kongens Lyngby, Denmark
²Corti AI, Copenhagen, Denmark. Correspondence to: Jakob D. Havtorn <jdh@corti.ai>, Lars Maaløe <lm@corti.ai>.

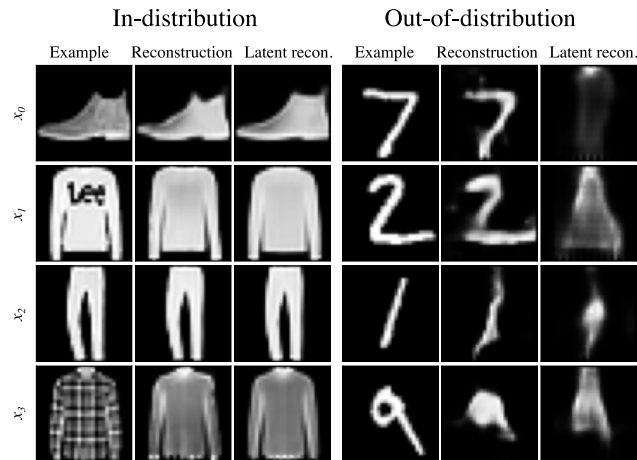


Figure 1. Reconstructions using a hierarchical VAE trained on FashionMNIST. Reconstruction quality of OOD data is comparable to in-distribution data, resulting in high likelihoods and poor OOD discrimination. By sampling the k bottom-most latent variables from the conditional prior distribution $p(\mathbf{z}_{\geq l} | \mathbf{z}_{> l})$ (latent reconstructions) instead of the approximate posterior $q(\mathbf{z}_{> l} | \mathbf{z}_{< l})$, the model reconstructs from the training distribution resulting in lower $p(\mathbf{x} | \mathbf{z})$ for OOD data.

OOD data. By directly modeling the training distribution, such models are expected to assign low likelihoods to OOD data as it originates from regions of little or no support under the learned density (Bishop, 1994). Recent advances in deep generative models (Kingma & Welling, 2014; Rezende et al., 2014; Oord et al., 2016b; Salimans et al., 2017; Kingma & Dhariwal, 2018) have enabled learning high quality generative models on complex data such as natural images, sequences including audio (Oord et al., 2016a) and graphs (Kipf & Welling, 2016). However, recent observations have brought into question the quality of the learned density estimates by showing that they often assign higher likelihoods to OOD data than to in-distribution data (Nalisnick et al., 2019a; Choi et al., 2019). Many complex data distributions can be explained to a large degree by low-level features, e.g. edges in images. However, such features do not explain high-level semantics of the data and may inhibit OOD detection (Ren et al., 2019; Nalisnick et al., 2019a)

In this paper, we examine the failure cases of deep generative models on OOD detection tasks within the context of hierarchical VAEs, and make the following contributions:

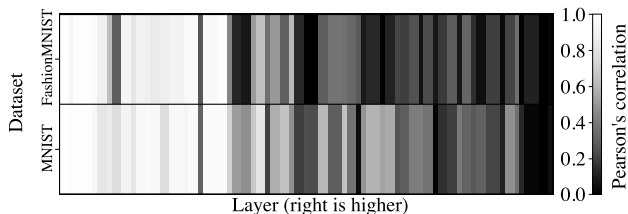


Figure 2. Absolute correlations between data representations in all layers of the inference network of a hierarchical VAE trained on FashionMNIST and of another trained on MNIST. We compute the correlation between the representations of the two different models given the same data, FashionMNIST (top) and MNIST (bottom).

- (i) We provide evidence that the root cause of OOD failures is that learned low-level features generalize well across datasets and dominate the estimated likelihoods.
- (ii) We then propose a fast, scalable, and fully unsupervised likelihood-ratio score for OOD detection that is explicitly developed to ensure that data should be in-distribution across all feature levels, which prevents the low-level features from dominating.
- (iii) With the likelihood-ratio score, we demonstrate state-of-the-art performance across a wide range of known OOD failure cases.

2. Why does OOD detection fail?

The inability to detect out-of-distribution data with deep generative models is surprising. Before the advent of deep generative models, this was not considered a major issue for probabilistic models (Bishop, 1994). Is the failure due to increased model flexibility, overfitting or something different?

Deep learning models are generally believed to form hierarchies of representations that range from low-level features to more conceptual ones related to semantics (Bengio et al., 2013). This has also been observed within deep generative models (Maaløe et al., 2019; Child, 2021). For image data there is a trend that the low-level features are quite similar across models (edge detectors, etc.), which raises the question to which extend such features are relevant when detecting OOD data, also suggested by (Nalisnick et al., 2019a). To investigate, we train two hierarchical VAEs (subsection 3.2) on FashionMNIST and MNIST, respectively, and compute the between-models correlation of the extracted features of in-distribution data and OOD data. The result appears in Figure 2. We observe that features extracted in the early layers (low-level features) correlate strongly between the two models, and that this correlation drops as we get into later layers. This suggests that low-level features do not carry much information for OOD detection.

To shed further light on the impact of semantic versus low-level features, we look at model reconstructions of images

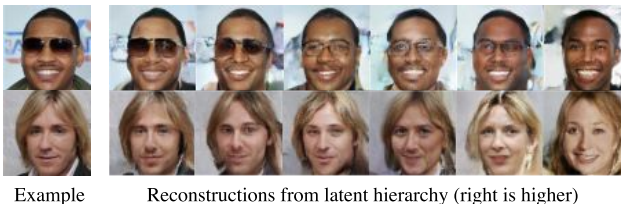


Figure 3. Reconstructions of in-distribution data (CelebA) of the BIVA model using higher latent variables (Maaløe et al., 2019). The higher the latent variable, the more the reconstructions fall into the mode of the learned distribution. It is more common to wear regular glasses than sunglasses but most common not to wear glasses at all. A man with long hair collapses into the mode of the more common long-haired woman.

with a hierarchical VAE (Figure 3). To study the feature hierarchy, we replace the inference distribution with the corresponding conditional prior in the first layers of the model to see what information is lost. We observe that as more layers rely on the prior, more details are lost. Sunglasses, which are uncommon, are first replaced by more common glasses, and then finally disappear. This suggests that as we fall back to the conditional priors of each layer, we are pushed closer to local modes of the modeled distribution.

Finally, we look at reconstructions of out-of-distribution data. Figure 1 illustrates that MNIST data is surprisingly well reconstructed by a hierarchical VAE trained on FashionMNIST. Similar results have been found elsewhere (Xiao et al., 2020). We repeat the previous experiment and replace inference distributions by their corresponding conditional prior, and now observe that reconstructions from higher latent layers become increasingly similar to the data on which the model was trained. The reliance on conditional priors seem to prevent accurate reconstruction of out-of-distribution data. Some details are lost on in-distribution data too, but the distinction between that and out-of-distribution data becomes more clear.

These observations lead to our main hypothesis. We hypothesize that the lowest latent variables in a hierarchical VAE learn generic features that can be used to describe a wide range of data. This enables the model to achieve high rates of compression, and hence high likelihoods, even on out-of-distribution data as long as the learned low-level features are appropriate. We further suggest that OOD data are in-distribution with respect to these low-level features, but not with respect to semantic ones.

3. Background and related work

3.1. Variational autoencoders

The variational autoencoder (VAE) (Kingma & Welling, 2014; Rezende et al., 2014) is a framework for constructing

deep generative models defined by an observed variable \mathbf{x} and a stochastic latent variable \mathbf{z} . Typically, a neural network with parameters θ is chosen to parameterize the generative distribution $p_\theta(\mathbf{x}, \mathbf{z}) = p_\theta(\mathbf{x}|\mathbf{z})p(\mathbf{z})$, where the prior $p(\mathbf{z})$ is commonly a standard Gaussian $\mathcal{N}(\mathbf{0}, \mathbf{I})$. The true posterior $p(\mathbf{z}|\mathbf{x})$ is generally not analytically tractable and is approximated by a variational distribution $q_\phi(\mathbf{z}|\mathbf{x})$ parameterized via another neural network with parameters ϕ . The approximate posterior $q_\phi(\mathbf{z}|\mathbf{x})$ is most often a diagonal covariance Gaussian. The model parameters θ and variational parameters ϕ are jointly optimized by maximizing the *evidence lower bound* (ELBO),

$$\log p_\theta(\mathbf{x}) \geq \mathbb{E}_{q_\phi(\mathbf{z}|\mathbf{x})} \left[\log \frac{p_\theta(\mathbf{x}, \mathbf{z})}{q_\phi(\mathbf{z}|\mathbf{x})} \right] \equiv \mathcal{L}(\mathbf{x}; \theta, \phi). \quad (1)$$

For brevity, we will denote $\mathcal{L}(\mathbf{x}; \theta, \phi)$ as $\mathcal{L}(\mathbf{x})$ or \mathcal{L} . The reparameterization trick is used to backpropagate gradients through the stochastic latent variables with low variance.

The VAE is defined with a single latent variable which limits the ability to learn a high likelihood representation of complex input distributions, e.g. natural images. There exist two complementary approaches to make the VAE more flexible: (i) model a more expressive prior distribution (Rezende & Mohamed, 2015; Kingma et al., 2016) and (ii) learn a deeper hierarchy of latent variables (Burda et al., 2016; Sønderby et al., 2016). We here focus on the latter.

3.2. Hierarchical variational autoencoders

Hierarchical VAEs are a family of probabilistic latent variable models which extends the basic VAE by introducing a hierarchy of L latent variables $\mathbf{z} = \mathbf{z}_1, \dots, \mathbf{z}_L$. The most common generative model is defined from the top down as $p_\theta(\mathbf{x}|\mathbf{z}) = p(\mathbf{x}|\mathbf{z}_1)p_\theta(\mathbf{z}_1|\mathbf{z}_2) \cdots p_\theta(\mathbf{z}_{L-1}|\mathbf{z}_L)$. The inference model can then be defined in two ways respectively referred to as *bottom-up* (Burda et al., 2016)

$$q_\phi(\mathbf{z}|\mathbf{x}) = q_\phi(\mathbf{z}_1|\mathbf{x}) \prod_{i=2}^L q_\phi(\mathbf{z}_i|\mathbf{z}_{i-1}) \quad (2)$$

and *top-down* (Sønderby et al., 2016)

$$q_\phi(\mathbf{z}|\mathbf{x}) = q_\phi(\mathbf{z}_L|\mathbf{x}) \prod_{i=L-1}^1 q_\phi(\mathbf{z}_i|\mathbf{z}_{i+1}). \quad (3)$$

Regardless of the choice of inference model, a hierarchical VAE is still trained using the ELBO (1).

Until recently, hierarchical VAEs gave inferior likelihoods compared to state-of-the-art autoregressive (Ho et al., 2019) and flow-based models (Salimans et al., 2017). This was changed by Maaløe et al. (2019), Vahdat & Kautz (2020), and Child (2021), which introduced complementary methods to extend the number of latent variables to a very deep hierarchy resulting in state-of-the-art likelihood performance.

In this paper we employ a simple hierarchical VAE with bottom-up inference paths and the more powerful BIVA variant with a bidirectional (top-down and bottom-up) inference

model (Maaløe et al., 2019). We employ skip connections between latent variables but omit them for brevity.

3.3. Out-of-distribution detection

So far, no reliable direct likelihood-based method has been found for fully unsupervised deep generative model OOD detection. A major line of work considers developing new scores that are more reliable than the likelihood. This includes the *typicality* test presented by Nalisnick et al. (2019b) which is an OOD detection test based on the typicality of a batch of potentially OOD examples. This approach however requires a batch of examples from the same class (OOD or not) which limits its practical applicability. In Ren et al. (2019), the *likelihood ratio* between a primary model and a background model was shown to be an effective score for OOD detection. However, to train the background model, the in-distribution data is perturbed via a data augmentation technique that is designed with knowledge about the confounding factors between the in-distribution data and the OOD data. Furthermore, it is tuned towards high performance on a known OOD dataset. Serrà et al. (2020) take a similar approach and attribute the failure to detect OOD data to the high influence of the input complexity on the likelihood and choose a generic lossless compression algorithm as the background model. Although this method gives good results, no single best choice of compression algorithm exists for all types of OOD data, and any particular choice encodes prior knowledge about the data into the detection method. Both these methods can be seen as correcting for low-level features of the OOD data being assigned high model likelihood by using a second model focused exclusively on these features.

Similar to these methods, the majority of the approaches to OOD detection make assumptions about the nature of the OOD data. The assumptions encompass using labels on the in-distribution data (Hendrycks & Gimpel, 2017; Liang et al., 2018; Alemi et al., 2018; Lee et al., 2018; Lakshminarayanan et al., 2017), examples of OOD data (Hendrycks et al., 2019), augmenting in-distribution data to mimic it (Ren et al., 2019), or assuming a certain data type (Serrà et al., 2020). Any of these assumptions encode implicit biases into the model about the attributes of OOD data which, in turn, might impair performance on truly unknown data examples (unknown unknowns).

While some of these methods achieve very good results on OOD detection with autoregressive models (Oord et al., 2016b; Salimans et al., 2017) and invertible flow-based models (Kingma & Dhariwal, 2018), it was recently shown that they can be much less effective for VAEs (Xiao et al., 2020) highlighting the need for a more reliable OOD score for VAEs. Although VAEs have the same failure cases as autoregressive and flow-based models, the caveat is that

the difference in the likelihood is generally not as big and reconstructions of OOD can be surprisingly good (Xiao et al., 2020). Xiao et al. (2020) alleviate this by refitting the inference network, as previously proposed by Cremer et al. (2018); Mattei & Frellsen (2018), to a potentially OOD example and measuring the so-called *likelihood regret*. However, refitting the inference network can be computationally expensive, especially for the large hierarchical VAEs that are used to model complex data (Maaløe et al., 2019; Vahdat & Kautz, 2020; Child, 2021). Furthermore, this scales poorly to large amounts of potentially OOD examples as the optimization is done per example.

A few methods have approached OOD detection in a completely unsupervised fashion (Maaløe et al., 2019; Choi et al., 2019; Xiao et al., 2020). The work of Maaløe et al. (2019) is the most related to ours. They introduce BIVA, a deep hierarchy of stochastic latent variables with a top-down and bottom-up inference model and achieve state-of-the-art likelihood scores. They also provide early results indicative that a looser likelihood bound may have value in OOD detection. In this paper, we provide an explanation of those results, and significantly improve upon them.

4. OOD detection with hierarchical VAEs

4.1. A bound for semantic OOD detection

If the first latent variable in the VAE hierarchy codes for a large part of the low-level features required to reconstruct the input with high accuracy, as exemplified in Figure 1-3, then $p_\theta(\mathbf{x}|\mathbf{z}_1)$ will be high for both in- and out-of-distribution data. Hence, any OOD detection capabilities based on the ELBO $\mathcal{L} = \mathbb{E}_{q_\phi(\mathbf{z}|\mathbf{x})}[\log p_\theta(\mathbf{x}|\mathbf{z}_1)] - D_{\text{KL}}(q_\phi(\mathbf{z}|\mathbf{x})||p(\mathbf{z}))$ from (1) relies on the KL-term for OOD detection. For a bottom-up hierarchical VAE, the KL-term $D_{\text{KL}}(q_\phi(\mathbf{z}|\mathbf{x})||p(\mathbf{z}))$ can be expressed by a hierarchical sum

$$\mathbb{E}_{q_\phi(\mathbf{z}|\mathbf{x})} \left[\sum_{i=1}^{L-1} \log \frac{p_\theta(\mathbf{z}_i|\mathbf{z}_{i+1})}{q_\phi(\mathbf{z}_i|\mathbf{z}_{i-1})} + \log \frac{p_\theta(\mathbf{z}_L)}{q_\phi(\mathbf{z}_L|\mathbf{z}_{L-1})} \right]. \quad (4)$$

In general, the absolute log-ratios grow with $\dim(\mathbf{z}_i)$ as the individual log probability terms are computed by summing over the dimensionality of \mathbf{z}_i . This means that the value of the KL-term is dominated by terms where \mathbf{z}_i is high-dimensional. Since hierarchical VAEs are generally constructed with a bottleneck type structure, the terms corresponding to latent variables towards the top of the hierarchy will have a vanishing influence on the value of the KL-term. However, as the semantic information most relevant for OOD detection has a tendency to be represented in the top-most latent variables, this makes OOD detection using the regular ELBO difficult, even for state-of-the-art models. This behavior has also been reported by Xiao et al. (2020).

To shift the ELBO from primarily being based on the approx-

imate posterior of the first latent variables to instead focus on the conditional prior, Maaløe et al. (2019) introduced another version of the ELBO defined as

$$\mathcal{L}^{>k} = \mathbb{E}_{p_\theta(\mathbf{z}_{\leq k}|\mathbf{z}_{>k})q_\phi(\mathbf{z}_{>k}|\mathbf{x})} \left[\log \frac{p_\theta(\mathbf{x}|\mathbf{z})p_\theta(\mathbf{z}_{>k})}{q_\phi(\mathbf{z}_{>k}|\mathbf{x})} \right] \quad (5)$$

where $k \in \{0, 1, \dots, L\}$ (see Appendix for the derivation). We note that $\mathcal{L}^{>0}$ is the regular ELBO (1) and that empirically we always observe that $\mathcal{L} \geq \mathcal{L}^{>k} \forall k$ although this need not hold in general. The core idea behind this variation on the ELBO is to sample the k lowest latent variables from the conditional prior $\mathbf{z}_1, \dots, \mathbf{z}_k \sim p_\theta(\mathbf{z}_{\leq k}|\hat{\mathbf{z}}_{>k})$ and only the $L - k$ highest from the approximate posterior $\mathbf{z}_{k+1}, \dots, \mathbf{z}_L \sim q_\phi(\mathbf{z}_{>k}|\mathbf{x})$. Importantly, this has the effect that the data likelihood $p(\mathbf{x}|\mathbf{z})$ is dependent on the approximate posterior through a latent variable \mathbf{z}_{k+1} different from \mathbf{z}_1 for all $k > 0$. Thereby, the likelihood can be evaluated with a reconstruction from each of the latent variables \mathbf{z}_k of the hierarchical VAE. Hence, we can now test how well the input \mathbf{x} is reconstructed from each latent variable. The notation $\mathcal{L}^{>k}$ highlights that for latent variables $\mathbf{z}_{>k}$, the bound is the regular ELBO while for the latent variables $\mathbf{z}_{\leq k}$, the bound is evaluated using the (conditional) prior rather than the approximate posterior as the proposal distribution.

For a different interpretation of the bound (5), consider that in an ideal VAE, the KL-divergence between q_ϕ and p_θ is zero. In practice, this indicates posterior collapse (Maaløe et al., 2017), but in the ideal case, it would mean that our approximate posterior has perfectly fitted the true model posterior, without collapsing into the prior, such that $q_\phi(\mathbf{z}_i|\mathbf{z}_{i-1}) = p_\theta(\mathbf{z}_i|\mathbf{z}_{i+1}) \forall i$ with $\mathbf{z}_0 \equiv \mathbf{x}$. In that case, (5) is equal to the ELBO for all values of k , $\mathcal{L} = \mathcal{L}^{>k} \forall k$.

4.2. A likelihood-ratio score for all feature levels

While the $\mathcal{L}^{>k}$ bound provides a score for performing semantic OOD detection, it still relies on the likelihood function (see equation (7) below), which is known to be problematic for OOD detection (section 3.3). To alleviate this, we phrase OOD detection as a likelihood ratio test of being *semantically* in-distribution. A standard likelihood ratio test (Buse, 1982) suggests to consider the ratio between the associated likelihoods, which we can approximate on a log-scale by the corresponding lower bounds \mathcal{L} and $\mathcal{L}^{>k}$,

$$LLR^{>k}(\mathbf{x}) = \mathcal{L}(\mathbf{x}) - \mathcal{L}^{>k}(\mathbf{x}). \quad (6)$$

Since, empirically, $\mathcal{L} \geq \mathcal{L}^{>k}$, the ratio is always positive as is standard for likelihood ratio tests. A low value of $LLR^{>k}(\mathbf{x})$ means that the ELBO and $\mathcal{L}^{>k}$ are almost equally tight for the data. On the contrary, a high value indicates that $\mathcal{L}^{>k}$ looser on the data than the ELBO, which indicates that the data may be OOD.

We can gather further insights about this score if we write the regular ELBO and the $\mathcal{L}^{>k}$ bounds in the exact form

that includes the intractable KL-divergence between the approximate and true posteriors,

$$\mathcal{L} = \log p_\theta(\mathbf{x}) - D_{\text{KL}}(q_\phi(\mathbf{z}|\mathbf{x})||p_\theta(\mathbf{z}|\mathbf{x})), \quad (7)$$

$$\mathcal{L}^{>k} = \log p_\theta(\mathbf{x}) - D_{\text{KL}}(p_\theta(\mathbf{z}_{\leq k}|\mathbf{z}_{>k})q_\phi(\mathbf{z}_{>k}|\mathbf{x})||p_\theta(\mathbf{z}|\mathbf{x})).$$

Subtracting these cancel out the two data likelihood terms $\log p_\theta(\mathbf{x})$ and only the KL-divergences from the approximate to the true posterior remain,

$$\begin{aligned} LLR^{>k}(\mathbf{x}) = & -D_{\text{KL}}(q_\phi(\mathbf{z}|\mathbf{x})||p_\theta(\mathbf{z}|\mathbf{x})) \\ & + D_{\text{KL}}(p_\theta(\mathbf{z}_{\leq k}|\mathbf{z}_{>k})q_\phi(\mathbf{z}_{>k}|\mathbf{x})||p_\theta(\mathbf{z}|\mathbf{x})). \end{aligned} \quad (8)$$

Hence, it is clear that compared to the likelihood bound $\mathcal{L}^{>k}$, this likelihood-ratio measures divergence exclusively in the latent space whereas $\mathcal{L}^{>k}$ includes the $\log p_\theta(\mathbf{x})$ term similar to the ELBO. Therefore, the $LLR^{>k}$ score should be an improved method for semantic OOD detection compared to $\mathcal{L}^{>k}$. Finally, it can be noted that if we replace the regular ELBO \mathcal{L} (7) with the strictly tighter importance weighted bound (Burda et al., 2016),

$$\mathcal{L}_S = \mathbb{E}_{q(\mathbf{z}|\mathbf{x})} \left[\log \frac{1}{N} \sum_{s=1}^S \frac{p(\mathbf{x}, \mathbf{z}^{(s)})}{q(\mathbf{z}^{(s)}|\mathbf{x})} \right], \quad (9)$$

then, in the limit $S \rightarrow \infty$, we have $\mathcal{L}_S \rightarrow \log p_\theta(\mathbf{x})$ and consequently the limit of the likelihood ratio reduces to

$$LLR_S^{>k}(\mathbf{x}) \xrightarrow{S} D_{\text{KL}}(p(\mathbf{z}_{\leq k}|\mathbf{z}_{>k})q(\mathbf{z}_{>k}|\mathbf{x})||p(\mathbf{z}|\mathbf{x})). \quad (10)$$

In practice, this limit is well-approximated for a finite S .

5. Experimental setup

Tasks: We follow existing literature (Nalisnick et al., 2019a; Hendrycks et al., 2019) and evaluate our method by setting up OOD detection tasks from FashionMNIST (Xiao et al., 2017) to MNIST (LeCun et al., 1998) and from CIFAR10 (Krizhevsky, 2009) to SVHN (Netzer et al., 2011). For each experiment we train our model on the train split of the former dataset and test its ability to recognize the test split of the latter dataset as OOD from the test split of the former dataset. We use the standard train/test splits for the datasets. More details on the datasets can be found in the Appendix.

Models: For each OOD task, we train a simple bottom-up hierarchical VAE with L stochastic layers which we will refer to as "HVAE". To alleviate posterior collapse we include skip-connections that connect \mathbf{z}_i to \mathbf{z}_{i+2} for $i \in \{0, L-2\}$ and $\mathbf{z}_0 \equiv \mathbf{x}$ in both the inference and generative models (Dieng et al., 2019) and employ the *free bits* scheme with $\lambda = 2$ (Kingma et al., 2016). We use weight-normalization (Salimans & Kingma, 2016) on all weights and residual networks in the deterministic paths. A graphical representation of this model can be seen in Figure 4. We use a

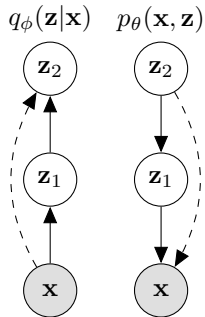


Figure 4. The inference and generative models, q_ϕ and p_θ , for an $L = 2$ layered bottom-up hierarchical VAE as the one used in our experiments. Dashed lines indicate deterministic skip connections which are employed in both networks. Skip connections are found to be useful for optimizing latent variable models (Dieng et al., 2019; Maaløe et al., 2019).

Bernoulli output distribution for FashionMNIST/MNIST and a discretized mixture of logistics output distribution (Salimans et al., 2017) for CIFAR10/SVHN. We use $L = 3$ for grey-scale images and $L = 4$ for natural images. For CIFAR/SVHN, we also train a BIVA model (Maaløe et al., 2019) with $L = 10$ and similar configuration as used by the original paper¹. We implement our models in PyTorch (Paszke et al., 2017). Full model details are in the Appendix.

Baselines: We group baselines into those that use prior knowledge about OOD data, ones that use labels associated with the in-distribution data and purely unsupervised approaches that do not make such assumptions. Our method falls into the latter category. For more information on each baseline, we refer to the original literature.

Evaluation: Following previous work (Hendrycks & Gimpel, 2017; Hendrycks et al., 2019; Alemi et al., 2018; Ren et al., 2019; Choi et al., 2019) we use the threshold-independent evaluation metrics of Area Under the Receiver Operator Characteristic (AUROC \uparrow), Area Under the Precision Recall Curve (AUPRC \uparrow) and False Positive Rate at 80% true positive rate (FPR80 \downarrow) where the arrow indicates the direction of improvement. Note that these metrics are only computable given examples of OOD data but faced with truly OOD data (unknown unknowns), there are many ways to select thresholds to use in practice e.g. as the one that yields a specific tolerable false positive rate on the in-distribution test data. To compute the metrics, we use an equal number of samples from the in-distribution and OOD datasets by including all examples in the smallest of the two sets and randomly sampling equally many from the larger. We compute the $LLR^{>k}$ score with one and S importance samples denoted by $LLR_S^{>k}$.

Selection of k : To determine whether an example is OOD in practice, the value of $LLR^{>k}$ is computed on the in-distribution test set for all k and the resulting empirical distribution is used as reference. If for any value of k , the $LLR^{>k}$ score of a new input differs significantly from the empirical distribution, it is regarded OOD. If it differs

¹github.com/larsmaaloe/BIVA and github.com/vlievin/biva-pytorch

Hierarchical VAEs Know What They Don't Know

Method	Dataset	Avg. bits/dim			
		$\log p(x)$	$\mathcal{L}^{>1}$	$\mathcal{L}^{>2}$	$\mathcal{L}^{>3}$
Trained on FashionMNIST					
Glow	FashionMNIST	2.96	-	-	-
	MNIST	1.83	-	-	-
HVAE (Ours)	FashionMNIST	0.420	0.476	0.579	-
	MNIST	0.317	0.601	0.881	-
Trained on CIFAR10					
Glow	CIFAR10	3.46	-	-	-
	SVHN	2.39	-	-	-
HVAE (Ours)	CIFAR10	3.74	17.8	54.3	75.7
	SVHN	2.62	10.2	64.0	93.9
BIVA (Ours)	CIFAR10	3.46	8.74	19.7	37.3
	SVHN	2.35	6.62	25.1	59.0

Table 1. Average bits per dimension of different datasets for models trained on FashionMNIST and CIFAR10. For the hierarchical models we include the $\mathcal{L}^{>k}$ bounds. The likelihoods of training and test splits of the in-distribution data are all cases close. Since we train on dynamically binarized FashionMNIST, our bits/dim are smaller than for Glow. As k is increased for the $\mathcal{L}^{>k}$ bound, the bound gets looser but the model eventually assigns higher likelihood to the in distribution data than to the OOD data. Glow refers to Kingma & Dhariwal (2018); Nalisnick et al. (2019a). BIVA refers to our implementation of Maaløe et al. (2019).

for multiple values of k , the value for which it differs the most is selected. In our experiments, we consider an entire dataset at a time and report the results of $LLR^{>k}$ with the value of k that yielded the highest AUROC \uparrow for that dataset in a threshold-free manner. In practice, slightly better performance may be achieved by choosing k per example. This would not exclude the use of batching in our method, since $LLR^{>k}$ is computed after the forward pass.

6. Results

The likelihoods for our trained models are in Table 1 alongside baseline results for in-distribution and OOD data. The main results of the paper on the OOD tasks can be seen along with comparisons to the baseline methods in Table 2. We note that for all our results, the value of the score ($\mathcal{L}^{>k}$ and $LLR^{>k}$) for the training and test splits of the in-distribution data was observed to have the same empirical distribution as within sampling error hence yielding an AUROC score of ≈ 0.5 as expected. Results on additional commonly used datasets are found in the Appendix.

6.1. Likelihood-based OOD detection

We first report the results of the different variations of the $\mathcal{L}^{>k}$ bound for OOD detection. We reconfirm the results of

¹Serrà et al. (2020) performs the best when high likelihoods are assigned to OOD data such that the overlap with in-distribution data is low. Performance is worse when the overlap is high, cf. Serrà et al. (2020, Table 1), as seen with complex images.

Method	AUROC \uparrow	AUPRC \uparrow	FPR80 \downarrow
FashionMNIST (in) / MNIST (out)			
Use prior knowledge of OOD			
Backgr. contrast. LR (PixelCNN) [1]	0.994	0.993	0.001
Backgr. contrast. LR (VAE) [7]	0.924	-	-
Binary classifier [1]	0.455	0.505	0.886
$p(\hat{y} x)$ with OOD as noise class [1]	0.877	0.871	0.195
$p(\hat{y} x)$ with calibration on OOD [1]	0.904	0.895	0.139
Input complexity (S , Glow) [9]	0.998	-	-
Input complexity (S , PixelCNN++) [9]	0.967	-	-
Input complexity (S , HVAE) (Ours)	-	-	-
Use in-distribution data labels y			
$p(\hat{y} x)$ [1], [2]	0.734	0.702	0.506
Entropy of $p(y x)$ [1]	0.746	0.726	0.448
ODIN [1, 3]	0.752	0.763	0.432
VIB [4, 7]	0.941	-	-
Mahalanobis distance, CNN [1]	0.942	0.928	0.088
Mahalanobis distance, DenseNet [5]	0.986	-	-
Ensemble, 20 classifiers [1, 6]	0.857	0.849	0.240
No OOD-specific assumptions			
WAIC, 5 models, PixelCNN [1]	0.221	0.401	0.911
WAIC, 5 models, Glow [7]	0.766	-	-
Likelihood regret [8]	0.988	-	-
$\mathcal{L}^{>0}$ + HVAE (ours)	0.268	0.363	0.882
$\mathcal{L}^{>1}$ + HVAE (ours)	0.593	0.591	0.658
$\mathcal{L}^{>2}$ + HVAE (ours)	0.712	0.750	0.548
$LLR^{>1}$ + HVAE (ours)	0.964	0.961	0.036
$LLR^{>2}_{250}$ + HVAE (ours)	0.984	0.984	0.013
CIFAR10 (in) / SVHN (out)			
Use prior knowledge of OOD			
Backgr. contrast. LR (PixelCNN) [1]	0.930	0.881	0.066
Backgr. contrast. LR (VAE) [8]	0.265	-	-
Outlier exposure [9]	0.984	-	-
Input complexity (S , Glow) [10]	0.950	-	-
Input complexity (S , PixelCNN++) [10]	0.929	-	-
Input complexity (S , HVAE) (Ours) [10] ²	0.833	0.855	0.344
Use in-distribution data labels y			
Mahalanobis distance [5]	0.991	-	-
No OOD-specific assumptions			
Likelihood regret [8]	0.875	-	-
$LLR^{>2}$ + HVAE (ours)	0.811	0.837	0.394
$LLR^{>2}$ + BIVA (ours)	0.891	0.875	0.172

Table 2. AUROC \uparrow , AUPRC \uparrow and FPR80 \downarrow for OOD detection for a FashionMNIST model using scores on the FashionMNIST test set as reference. HVAE (ours) refers to our hierarchical bottom-up VAE. BIVA (ours) refers to our implementation of the hierarchical BIVA model (Maaløe et al., 2019). [1] is (Ren et al., 2019), [2] is (Hendrycks & Gimpel, 2017), [3] is (Liang et al., 2018), [4] is (Aleami et al., 2018), [5] is (Lee et al., 2018), [6] is (Lakshminarayanan et al., 2017), [7] is (Choi et al., 2019), [8] is (Xiao et al., 2020), [9] is (Hendrycks et al., 2019), [10] is (Serrà et al., 2020).

Nalisnick et al. (2019a) by observing that our hierarchical latent variable models also assign higher $\mathcal{L}^{>0}$ to the OOD dataset in the FashionMNIST/MNIST and CIFAR10/SVHN cases resulting in an AUROC \uparrow inferior to random (Table 2). Switching the in-distribution data for the OOD data in both cases result in correctly detecting the OOD data; an asymmetry also reported by Nalisnick et al. (2019a). Figure 5a shows the density of $\mathcal{L}^{>0}$ in bits per dimension (Theis et al., 2016) by the model trained on FashionMNIST when evaluated on the FashionMNIST and MNIST test sets. We observe a high degree of overlap, with less separation of the OOD data compared to similar results of autoregressive and

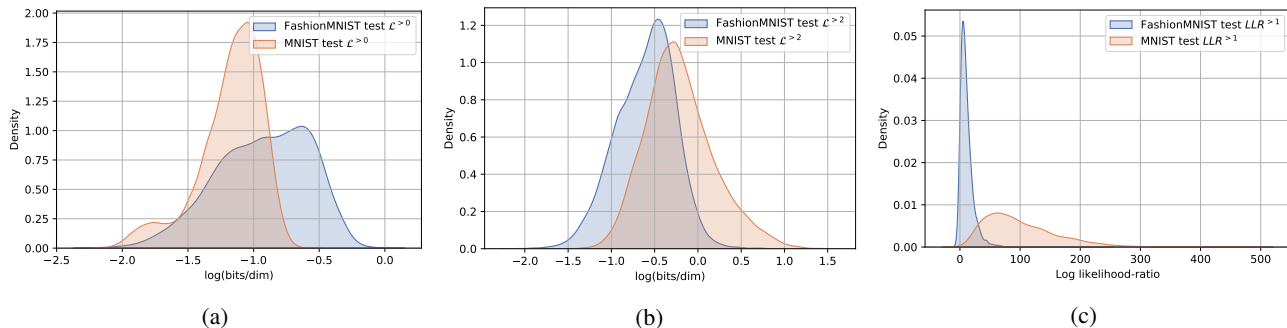


Figure 5. Empirical densities of FashionMNIST (in-distribution) and MNIST (OOD) using the raw likelihood (a), the $\mathcal{L}^{>2}$ bound (b) and the $LLR^{>1}$ score (c). All densities area computed using the HVAE model. For the regular likelihood MNIST is very clearly more likely on average than the FashionMNIST test data while with the $\mathcal{L}^{>2}$ bound separation is better but significant overlap remains. The $LLR^{>1}$ provides a high degree of separation. Likelihoods are reported in units of the natural log of the number of bits per dimension.

flow-based models, like Xiao et al. (2020).

We then evaluate the looser $\mathcal{L}^{>k}$ (5) for $k \in \{1, L\}$. Figure 5b shows the result for $\mathcal{L}^{>2}$, which yielded the highest AUCROC \uparrow , only slightly better than random. Like Maaløe et al. (2019), we see that increasing the value of k generally leads to improved OOD detection. However, we also observe that the two empirical distributions never cease to overlap. Importantly, depending on the OOD dataset, the amount of remaining overlap can be high which limits the discriminatory power of the likelihood-based $\mathcal{L}^{>k}$ bound. This is in-line with the pathological behavior of the raw likelihood of latent variable models when used for OOD detection (Xiao et al., 2020). Since a high degree of overlap also seems present in Maaløe et al. (2019), and we see the same problem for our BIVA model trained on CIFAR10, we do not expect this to be due to the less expressive HVAE.

6.2. Likelihood-ratio-based OOD detection

We now move to the likelihood ratio-based score. We find that $LLR^{>k}$ separates the OOD MNIST data from in-distribution FashionMNIST to a higher degree than the likelihood estimates as can be seen by the empirical densities of the score in Figure 5c. We note that the likelihood ratio between the ELBO and the $\mathcal{L}^{>k}$ bound provides the highest degree of separation of MNIST and FashionMNIST as measured by the AUCROC \uparrow for $k = 1$ smaller than L . This is not surprising since the value of k that provides the maximal separation to the reference in-distribution dataset need not be the one for which $\mathcal{LLR}^{>k}$ is overall maximal for the OOD dataset. We also visualize the ROC curves resulting from using the $LLR^{>k}$ score for OOD detection on both FashionMNIST/MNIST and CIFAR10/SVHN and compare it to the ROC curves resulting from the different $\mathcal{L}^{>k}$ bounds in Figures 6 and 7, respectively. On both datasets we see significantly better discriminatory performance when using the $LLR^{>k}$ score.

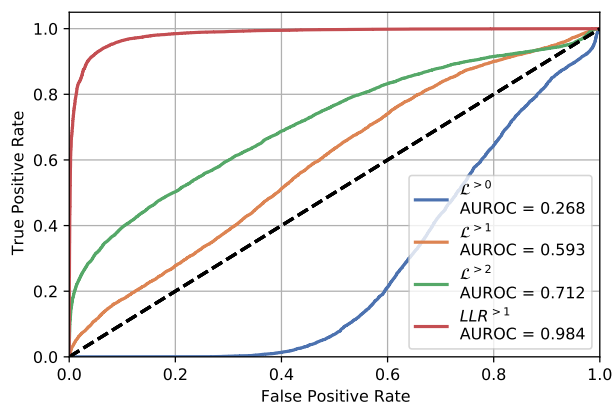


Figure 6. ROC curves with AUROC score for detecting MNIST as OOD with the HVAE model trained on FashionMNIST. A ROC curve is plotted for each of the $\mathcal{L}^{>k}$ bounds including the ELBO along with one for the best-performing log likelihood-ratio $LLR^{>1}$.

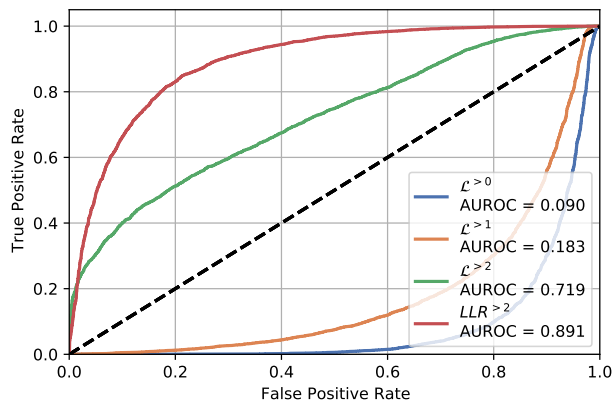


Figure 7. ROC curves with AUROC score for detecting SVHN as OOD with the BIVA model trained on CIFAR10. A ROC curve is plotted for each of the $\mathcal{L}^{>k}$ bounds including the ELBO along with one for the best-performing log likelihood-ratio $LLR^{>2}$.

Table 2 shows that BIVA improves upon the HVAE model for OOD detection on CIFAR while Table 1 shows that the BIVA model also improves upon the HVAE in terms of likelihood. We hypothesize that models larger than our implementation of BIVA, with better likelihood scores may perform even better (Maaløe et al., 2019; Vahdat & Kautz, 2020; Child, 2021).

6.3. Comparison to baselines

Performance: Table 2 summarize our results compared to baselines based on the commonly used AUROC \uparrow , AUPRC \uparrow and FPR80 \downarrow metrics. Our method outperforms other generative model-based methods such as WAIC (Choi et al., 2019) with Glow model and performs similarly to the likelihood regret method of (Xiao et al., 2020). Furthermore, our method performs similarly to the background contrastive likelihood ratio method of Ren et al. (2019) on FashionMNIST/MNIST but contrary to the failure of that method on CIFAR10/SVHN reported by (Xiao et al., 2020), our method performs very well on this task too. Our approach outperforms all supervised approaches that use in-distribution labels or synthetic examples of OOD data derived from the in-distribution data including ODIN (Liang et al., 2018) and the predictive distribution of a classifier $p(\hat{y}|\mathbf{x})$ trained and evaluated in various ways (see Ren et al. (2019)).

Runtime: For a full evaluation of a single example across all feature levels of a model with L stochastic layers, our method requires $L - 1$ forward passes through the inference and generative networks as well as computing the likelihood ratio, of which the forward passes are dominant. For a typical forward pass that is linear in the input dimensionality, D , and the number of stochastic layers, L , this amounts to computation of $\mathcal{O}(DL)$. Compared to some related work that either requires an $M > 1$ sized batch of inputs of which either all or none are OOD (Nalisnick et al., 2019b) or cannot be applied to batches due to the required per-example optimization (Xiao et al., 2020), our method additionally is applicable to batches of any size that may consist of both OOD and in-distribution examples which provides drastic speed-ups via vectorization and parallelization. Furthermore, the method of Xiao et al. (2017) requires refitting the inference network of a VAE which can be computationally demanding. Compared to the likelihood ratio proposed in Ren et al. (2019), our method requires training only a single model on a single dataset.

7. Discussion

Deep generative models are state-of-the-art density estimators, but the OOD failures reported in recent years have raised concerns about the limitations of such density estimates. Recent work on improving OOD detection has largely sidestepped this concern by relying on additional

assumptions that strictly should not be needed for models with explicit likelihoods. While the engineering challenge of building reliable OOD detection schemes is important, it is of more fundamental importance to understand *why* the naive likelihood test fails. We have provided evidence that low-level features of the neural nets dominate the likelihood, which gives a *cause* to the *why*. The fact that a simple score for measuring the importance of semantic features yield state-of-the-art results on OOD detection without access to additional information gives validity to our hypothesis.

The findings from, amongst others, Nalisnick et al. (2019a); Serrà et al. (2020) have a clear relation to information theory and compression. Semantically complex in-distribution data yields models with diverse low-level feature sets that enable generalization across datasets. Simpler datasets can only yield models with less diverse low-level feature sets compared to complex training data. Hence, there can be an asymmetry where the likelihoods of simple OOD data can be high for a model trained on complex data, but not the other way around. Loosely put, the minimal number of bits required to losslessly compress data sampled from some distribution is the entropy of the generating process (Shannon, 1948; MacKay, 2003). Townsend et al. (2019) recently showed that VAEs can be used for lossless compression at rates superior to more generic algorithms.

We also note that since the hierarchical VAE is a probabilistic graphical latent variable model, it lends itself very naturally to manipulation at the feature level (Kingma et al., 2014; Maaløe et al., 2016; 2017). This property sets it apart from other generative models that do not explicitly define such a hierarchy of features. This in turn enables reliable OOD detection with our methodology while making no explicit assumptions about the nature of OOD data and only using a single model. This has not been achieved with autoregressive or flow-based models.

8. Conclusion

In this paper we study unsupervised out-of-distribution detection using hierarchical variational autoencoders. We provide evidence that highly generalizable low-level features contribute greatly to estimated likelihoods resulting in poor OOD detection performance. We proceed to develop a likelihood-ratio based score for OOD detection and define it to explicitly ensure that data must be in-distribution across all feature levels to be regarded in-distribution. This ratio is mathematically shown to perform OOD detection in the latent space of the model, removing the reliance on the troublesome input-space likelihood. We point out that contrary to much recent literature on OOD detection, our approach is fully unsupervised and does not make assumptions about the nature of OOD data. Finally, we demonstrate state-of-the-art performance on a wide range of OOD failure cases.

Acknowledgements

This research was partially funded by the Danish Innovation Fund via the Industrial PhD Programme (grant no. 0153-00167B). JF and SH were funded in part by the Novo Nordisk Foundation (grant no. 0062606) via the Center for Basic Machine Learning Research in Life Science (MLLS, <https://www.mlls.dk>). SH was further funded by VILLUM FONDEN (15334) and the European Research Council (ERC) under the European Union's Horizon 2020 research and innovation programme (grant agreement no. 757360).

References

- Alemi, A. A., Fischer, I., and Dillon, J. V. Uncertainty in the Variational Information Bottleneck. *arXiv:1807.00906*, July 2018. URL <http://arxiv.org/abs/1807.00906>.
- Bengio, Y., Courville, A. C., and Vincent, P. Representation learning: A review and new perspectives. *IEEE Transactions on Pattern Analysis and Machine Intelligence*, 35(8): 1798–1828, 2013. doi: 10.1109/TPAMI.2013.50. URL <https://doi.org/10.1109/TPAMI.2013.50>.
- Bishop, C. M. Novelty Detection and Neural-Network Validation. *IEE Proceedings - Vision, Image and Signal Processing*, 141(4):217–222, 1994. ISSN 1350245x, 13597108. doi: 10.1049/ip-vis:19941330.
- Bulatov, Y. notMNIST dataset, September 2011. URL <http://yaroslavvb.blogspot.com/2011/09/notmnist-dataset.html>.
- Burda, Y., Grosse, R., and Salakhutdinov, R. R. Importance Weighted Autoencoders. In *Proceedings of the 4th International Conference on Learning Representations (ICLR)*, pp. 8, San Juan, Puerto Rico, 2016. URL <https://arxiv.org/abs/1509.00519>.
- Buse, A. The likelihood ratio, Wald, and Lagrange multiplier tests: An expository note. *The American Statistician*, 36(3a):153–157, 1982.
- Child, R. Very Deep VAEs Generalize Autoregressive Models and Can Outperform Them on Images. In *Proceedings of the 9th International Conference on Learning Representations (ICLR)*, 2021. URL <https://arxiv.org/pdf/2011.10650.pdf>.
- Choi, H., Jang, E., and Alemi, A. A. WAIC, but Why? Generative Ensembles for Robust Anomaly Detection. *arXiv:1810.01392*, May 2019. URL <http://arxiv.org/abs/1810.01392>.
- Clanuwat, T., Bober-Irizar, M., Kitamoto, A., Lamb, A., Yamamoto, K., and Ha, D. Deep Learning for Classical Japanese Literature. *arXiv:1812.01718 [cs, stat]*, December 2018. doi: 10.20676/00000341. URL <http://arxiv.org/abs/1812.01718>. arXiv: 1812.01718.
- Cremer, C., Li, X., and Duvenaud, D. Inference Suboptimality in Variational Autoencoders. In Dy, J. and Krause, A. (eds.), *Proceedings of the 35th International Conference on Machine Learning (ICML)*, volume 80 of *Proceedings of machine learning research*, pp. 1078–1086, Stockholm, Sweden, July 2018. PMLR. URL <http://proceedings.mlr.press/v80/cremer18a.html>.
- DeVries, T. and Taylor, G. W. Learning Confidence for Out-of-Distribution Detection in Neural Networks. *arXiv:1802.04865*, February 2018. URL <http://arxiv.org/abs/1802.04865>.
- Dieng, A. B., Kim, Y., Rush, A. M., and Blei, D. M. Avoiding latent variable collapse with generative skip models. In Chaudhuri, K. and Sugiyama, M. (eds.), *Proceedings of the 22nd International Conference on Artificial Intelligence and Statistics (AISTATS)*, volume 89, pp. 2397–2405, Naha, Okinawa, Japan, 2019. PMLR. URL <http://proceedings.mlr.press/v89/dieng19a.html>.
- Fukushima, K. Neocognitron: A Self-organizing Neural Network Model for a Mechanism of Pattern Recognition Unaffected by Shift in Position. *Biological Cybernetics*, 36(4):193–202, 1980.
- Goodfellow, I. J., Shlens, J., and Szegedy, C. Explaining and harnessing adversarial examples. In Bengio, Y. and LeCun, Y. (eds.), *Proceedings of the 3rd International Conference on Learning Representations (ICLR)*, San Diego, CA, USA, 2015. URL <http://arxiv.org/abs/1412.6572>.
- Hendrycks, D. and Gimpel, K. A Baseline for Detecting Misclassified and Out-of-Distribution Examples in Neural Networks. In *Proceedings of the 5th International Conference on Learning Representations (ICLR)*, Toulon, France, 2017. URL <http://arxiv.org/abs/1610.02136>. arXiv: 1610.02136.
- Hendrycks, D., Mazeika, M., and Dietterich, T. G. Deep anomaly detection with outlier exposure. In *Proceedings of the 7th International Conference on Learning Representations (ICLR)*, New Orleans, LA, USA, 2019. URL <https://openreview.net/forum?id=HyxCxhRcY7>.
- Ho, J., Chen, X., Srinivas, A., Duan, Y., and Abbeel, P. Flow++: Improving Flow-Based Generative Models with Variational Dequantization and Architecture Design. In

- Proceedings of the 36th International Conference on Machine Learning (ICML)*, pp. 9, Long Beach, CA, USA, 2019. URL <http://proceedings.mlr.press/v97/hol19a/hol19a.pdf>.
- Ioffe, S. and Szegedy, C. Batch Normalization: Accelerating Deep Network Training by Reducing Internal Covariate Shift. In *Proceedings of the International Conference on Machine Learning (ICML)*, Lille, France, 2015. URL <http://arxiv.org/abs/1502.03167>. arXiv: 1502.03167.
- Kingma, D. P. and Ba, J. L. Adam: A Method for Stochastic Optimization. *arXiv preprint*, December 2014. URL <http://arxiv.org/abs/1412.6980>. arXiv: 1412.6980.
- Kingma, D. P. and Dhariwal, P. Glow: Generative Flow with Invertible 1×1 Convolutions. In *Proceedings of the 32nd Conference on Neural Information Processing Systems (NeurIPS)*, pp. 10, Montréal, Canada, 2018.
- Kingma, D. P. and Welling, M. Auto-Encoding Variational Bayes. In *Proceedings of the 2nd International Conference on Learning Representations (ICLR)*, Banff, AB, Canada, 2014. URL <http://arxiv.org/abs/1312.6114>. arXiv: 1312.6114.
- Kingma, D. P., Rezende, D. J., Mohamed, S., and Welling, M. Semi-Supervised Learning with Deep Generative Models. In *Proceedings of the 28th International Conference on Neural Information Processing Systems (NeurIPS)*, Montréal, Quebec, Canada, June 2014. URL <http://arxiv.org/abs/1406.5298>. arXiv: 1406.5298.
- Kingma, D. P., Salimans, T., Jozefowicz, R., Chen, X., Sutskever, I., and Welling, M. Improved variational inference with inverse autoregressive flow. In *Proceedings of the 30th International Conference on Neural Information Processing Systems (NeurIPS)*, NIPS'16, pp. 4743–4751, Barcelona, Spain, 2016. ISBN 978-1-5108-3881-9. URL <http://arxiv.org/abs/1606.04934>.
- Kipf, T. N. and Welling, M. Variational Graph Auto-Encoders. *arXiv:1611.07308*, November 2016. URL <http://arxiv.org/abs/1611.07308>.
- Krizhevsky, A. *Learning Multiple Layers of Features from Tiny Images*. PhD thesis, University of Toronto, 2009. arXiv: 1011.1669v3 ISBN: 9788578110796 ISSN: 1098-6596.
- Lake, B. M., Salakhutdinov, R., and Tenenbaum, J. B. Human-level concept learning through probabilistic program induction. *Science*, 350(6266):1332–1338, 2015. ISSN 0036-8075. doi: 10.1126/science.aab3050. URL <https://science.sciencemag.org/content/350/6266/1332>.
- Lakshminarayanan, B., Pritzel, A., and Blundell, C. Simple and Scalable Predictive Uncertainty Estimation using Deep Ensembles. In *In Proceedings of the 31st Conference on Neural Information Processing Systems (NeurIPS)*, Long Beach, CA, USA, 2017. URL <http://arxiv.org/abs/1612.01474>.
- LeCun, Y., Huang, F., and Bottou, L. Learning methods for generic object recognition with invariance to pose and lighting. In *IEEE Computer Society Conference on Computer Vision and Pattern Recognition (CVPR 2004)*, volume 2, pp. II–104 Vol.2, 2004.
- LeCun, Y. A., Bottou, L., Bengio, Y., and Haffner, P. Gradient-based learning applied to document recognition. *Proceedings of the IEEE*, 86(11):2278–2323, 1998.
- Lee, K., Lee, K., Lee, H., and Shin, J. A Simple Unified Framework for Detecting Out-of-Distribution Samples and Adversarial Attacks. In *Proceedings of the 32nd Conference on Neural Information Processing Systems (NeurIPS)*, pp. 11, Montréal, Quebec, Canada, 2018. URL <https://papers.nips.cc/paper/2018/file/abdeb6f575ac5c6676b747bca8d09cc2-Paper.pdf>.
- Liang, S., Li, Y., and Srikant, R. Enhancing the reliability of out-of-distribution image detection in neural networks. In *Proceedings of the 6th International Conference on Learning Representations (ICLR)*, Vancouver, Canada, 2018. URL <https://openreview.net/forum?id=H1VGkIxRZ>.
- Maaløe, L., Sønderby, C. K., Sønderby, S. K., and Winther, O. Auxiliary deep generative models. In Balcan, M. F. and Weinberger, K. Q. (eds.), *Proceedings of the 33rd international conference on machine learning*, volume 48 of *Proceedings of machine learning research*, pp. 1445–1453, New York, New York, USA, June 2016. PMLR. URL <http://proceedings.mlr.press/v48/maaloe16.html>.
- Maaløe, L., Fraccaro, M., and Winther, O. Semi-Supervised Generation with Cluster-aware Generative Models. *arXiv:1704.00637*, April 2017. URL <http://arxiv.org/abs/1704.00637>.
- Maaløe, L., Fraccaro, M., Liévin, V., and Winther, O. BIVA: A Very Deep Hierarchy of Latent Variables for Generative Modeling. In *Proceedings of the 32nd Conference on Neural Information Processing Systems (NeurIPS)*, pp. 6548–6558, Vancouver, Canada, February 2019. URL <http://arxiv.org/abs/1902.02102>. arXiv: 1902.02102.

- MacKay, D. J. C. *Information theory, inference, and learning algorithms*. Cambridge University Press, 1 edition, 2003. ISBN 978-0-521-64298-9.
- Mattei, P.-A. and Frellsen, J. Refit your encoder when new data comes by. In *3rd NeurIPS Workshop on Bayesian Deep Learning*, 2018.
- Muirhead, R. J. *Aspects of multivariate statistical theory*, volume 197. John Wiley & Sons, 2009.
- Nair, V. and Hinton, G. E. Rectified linear units improve restricted boltzmann machines. In *Proceedings of the 27th International Conference on Machine Learning (ICML 2011)*, pp. 807–814, Haifa, Israel, 2010. URL <https://icml.cc/Conferences/2010/papers/432.pdf>.
- Nalisnick, E., Matsukawa, A., Teh, Y. W., Gorur, D., and Lakshminarayanan, B. Do Deep Generative Models Know What They Don't Know? In *Proceedings of the 7th International Conference on Learning Representations (ICLR)*, New Orleans, LA, USA, 2019a. URL <http://arxiv.org/abs/1810.09136>. arXiv: 1810.09136.
- Nalisnick, E., Matsukawa, A., Teh, Y. W., and Lakshminarayanan, B. Detecting Out-of-Distribution Inputs to Deep Generative Models Using Typicality. *arXiv:1906.02994*, pp. 15, 2019b. URL <https://arxiv.org/abs/1906.02994>.
- Netzer, Y., Wang, T., Coates, A., Bissacco, A., Wu, B., and Ng, A. Y. Reading Digits in Natural Images with Unsupervised Feature Learning. In *NeurIPS Workshop on Deep Learning and Unsupervised Feature Learning 2011*, 2011. URL http://ufldl.stanford.edu/housenumbers/nips2011_housenumbers.pdf.
- Nguyen, A., Yosinski, J., and Clune, J. Deep neural networks are easily fooled: High confidence predictions for unrecognizable images. In *Proceedings of the IEEE Conference on Computer Vision and Pattern Recognition (CVPR)*, volume 07-12-June, pp. 427–436, 2015. ISBN 978-1-4673-6964-0. doi: 10.1109/CVPR.2015.7298640.
- Oord, A. v. d., Dieleman, S., Zen, H., Simonyan, K., Vinyals, O., Graves, A., Kalchbrenner, N., Senior, A., and Kavukcuoglu, K. WaveNet: A Generative Model for Raw Audio. In *In Proceedings of the 9th ISCA Speech Synthesis Workshop*, Sunnyval, CA, USA, September 2016a. URL <http://arxiv.org/abs/1609.03499>.
- Oord, A. v. d., Kalchbrenner, N., and Kavukcuoglu, K. Pixel Recurrent Neural Networks. In *Proceedings of the 33rd International Conference on Machine Learning (ICML)*, New York, NY, USA, August 2016b. Journal of Machine Learning. URL <http://arxiv.org/abs/1601.06759>. arXiv: 1601.06759.
- Paszke, A., Chanan, G., Lin, Z., Gross, S., Yang, E., Antiga, L., and Devito, Z. Automatic differentiation in PyTorch. In *In Proceedings of the 31st Conference on Neural Information Processing Systems (NeurIPS)*, 2017. URL <https://pytorch.org/>.
- Ren, J., Liu, P. J., Fertig, E., Snoek, J., Poplin, R., Depristo, M., Dillon, J., and Lakshminarayanan, B. Likelihood Ratios for Out-of-Distribution Detection. In *Proceedings of the 33rd International Conference on Neural Information Processing Systems (NeurIPS)*, pp. 12, Vancouver, Canada, 2019. URL <https://papers.nips.cc/paper/2019/file/1e79596878b2320cac26dd792a6c51c9-Paper.pdf>.
- Rezende, D. J. and Mohamed, S. Variational Inference with Normalizing Flows. In *Proceedings of the 32nd International Conference on Machine Learning (ICML)*, Lille, France, 2015. URL <http://arxiv.org/abs/1505.05770>.
- Rezende, D. J., Mohamed, S., and Wierstra, D. Stochastic Backpropagation and Approximate Inference in Deep Generative Models. In *Proceedings of Machine Learning Research*, volume 32, pp. 1278–1286, Beijing, China, January 2014. PMLR. URL <http://proceedings.mlr.press/v32/rezende14.pdf>. arXiv: 1401.4082.
- Salimans, T. and Kingma, D. P. Weight Normalization: A Simple Reparameterization to Accelerate Training of Deep Neural Networks. In *Proceedings of the 30th Conference on Neural Information Processing Systems (NeurIPS)*, Barcelona, Spain, February 2016. URL <http://arxiv.org/abs/1602.07868>.
- Salimans, T., Karpathy, A., Chen, X., and Kingma, D. P. PixelCNN++: Improving the PixelCNN with Discretized Logistic Mixture Likelihood and Other Modifications. In *Proceedings of the 5th International Conference on Learning Representations (ICLR)*, Toulon, France, April 2017. URL <http://arxiv.org/abs/1701.05517>.
- Serrà, J., Álvarez, D., Gómez, V., Slizovskaia, O., Núñez, J. F., and Luque, J. Input complexity and out-of-distribution detection with likelihood-based generative models. In *Proceedings of the 8th International Conference on Learning Representations (ICLR)*, Addis Ababa, Ethiopia, 2020. URL <https://openreview.net/forum?id=SyxIWpVYvr>.

- Shannon, C. E. A Mathematical Theory of Communication. *The Bell System Technical Journal*, 27(July 1948):379–423, 1948. ISSN 07246811. doi: 10.1145/584091.584093. arXiv: chao-dyn/9411012 ISBN: 0252725484.
- Sønderby, C. K., Raiko, T., Maaløe, L., Sønderby, S. K., and Winther, O. Ladder Variational Autoencoders. In *Proceedings of the 29th Conference on Neural Information Processing Systems (NeurIPS)*, Barcelona, Spain, December 2016. URL <http://arxiv.org/abs/1602.02282>. arXiv: 1602.02282.
- Theis, L., Oord, A. v. d., and Bethge, M. A note on the evaluation of generative models. In *Proceedings of the 4th International Conference on Learning Representations (ICLR)*, San Juan, Puerto Rico, May 2016. URL <http://arxiv.org/abs/1511.01844>.
- Townsend, J., Bird, T., and Barber, D. Practical Lossless Compression With Latent Variables Using Bits Back Coding. In *7th International Conference on Learning Representations (ICLR)*, pp. 13, New Orleans, LA, USA, 2019.
- Vahdat, A. and Kautz, J. NVAE: A Deep Hierarchical Variational Autoencoder. In *34th Conference on Neural Information Processing Systems (NeurIPS)*, Virtual, July 2020. URL <http://arxiv.org/abs/2007.03898>. arXiv: 2007.03898.
- Xiao, H., Rasul, K., and Vollgraf, R. Fashion-MNIST: a Novel Image Dataset for Benchmarking Machine Learning Algorithms. *arXiv:1708.07747*, 2017. URL <http://arxiv.org/abs/1708.07747>.
- Xiao, Z., Yan, Q., and Amit, Y. Likelihood Regret: An Out-of-Distribution Detection Score for Variational Auto-Encoder. In *Proceedings of the 33rd Conference on Neural Information Processing Systems (NeurIPS)*, Virtual, 2020. URL <https://proceedings.neurips.cc/paper/2020/hash/eddea82ad2755b24c4e168c5fc2ebd40-Abstract.html>.

A. Datasets

Table 3 lists the datasets used in the paper. We use the predefined train/test splits for the datasets.

For SmallNORB and Omniglot we resize the original grey-scale images to 28×28 with ordinary bi-linear interpolation. For each of these datasets, we also create a version where the grey-scale is inverted. We do this because, the overall white nature of the images tends to make detecting them as OOD from FashionMNIST artificially easy. The inversion is done via the simple transformation $\mathbf{x}_{\text{inverted}} = 255 - \mathbf{x}_{\text{original}}$ since images are encoded as 8 bit unsigned integers.

Dataset	Dimensionality	Examples
FashionMNIST (Xiao et al., 2017)	$28 \times 28 \times 1$	70,000
MNIST (LeCun et al., 1998)	$28 \times 28 \times 1$	70,000
notMNIST (Bulatov, 2011)	$28 \times 28 \times 1$	547,838
KMNIST (Clanuwat et al., 2018)	$28 \times 28 \times 1$	70,000
Omniglot (Lake et al., 2015)	$28 \times 28 \times 1$	32,460
SmallNORB (LeCun et al., 2004)	$28 \times 28 \times 1$	97,200
CIFAR10 (Krizhevsky, 2009)	$32 \times 32 \times 3$	60,000
SVHN (Netzer et al., 2011)	$32 \times 32 \times 3$	99,289

Table 3. Overview of the used datasets.

B. Model details

In Table 4 we specify the hyperparameters used when training our models.

B.1. Hierarchical VAE

Our Hierarchical VAE (HVAE) model uses bottom-up inference and top-down generative paths as specified in the paper. For grey-scale images, the output is parameterized by a Bernoulli distribution while for natural images we use a Discretized Logistic Mixture (Salimans et al., 2017). The latent variables are parameterized by stochastic layers that output the mean and log-variance of a diagonal covariance Gaussian. The prior distribution on the top-most latent is a standard Gaussian. For grey-scale images, the first latent space is parameterized by a convolutional neural network and has dimensions $14 \times 14 \times 8$ interpreted as (height \times width \times latent dimension). The last two latent variables are parameterized by dense transformations with 16 and 8 units, respectively. For natural images, all latent variables are parameterized by convolutional neural networks and have dimensions $16 \times 16 \times 8$, $8 \times 8 \times 16$ and $4 \times 4 \times 32$, respectively for \mathbf{z}_1 , \mathbf{z}_2 and \mathbf{z}_3 .

Each stochastic layer is preceded by a deterministic transformation. For both grey-scale and natural images, each deterministic transformation consists of three residual blocks of the same type used by Maaløe et al. (2019). The structure

of a residual block is:

$$\mathbf{y} = \text{Conv}(\text{Act}(\text{Conv}_s(\text{Act}(\mathbf{x})))) + \mathbf{x},$$

where "Conv" refers to a same-padded convolution and "Act" to the activation function. Within a residual block, the first convolution always has stride 1 while the second convolution has stride s . In a deterministic transformation, any non-unit stride is performed in the third residual block. For grey-scale images, we stride by 2 in the first and second deterministic transformations but not the third. For natural images, we stride by 2 in all three deterministic blocks. In both cases, the first deterministic block uses a kernel size of 5 and the latter two a kernel of size 3. We use the ReLU activation function (Fukushima, 1980; Nair & Hinton, 2010).

Since the benefits and drawbacks of using batch normalization (Ioffe & Szegedy, 2015) in hierarchical VAEs is still the matter of some debate (Sønderby et al., 2016; Vahdat & Kautz, 2020; Child, 2021) we choose to use weight normalization (Salimans & Kingma, 2016) as in other work (Maaløe et al., 2019) and initialize the model using the originally proposed data-dependent initialization. To have the stochastic layers initialize to standard Gaussian distributions (zero mean, unit variance), with this initialization, we select the activation function for the variance as a Softplus,

$$\text{Softplus}(\mathbf{x}) = \frac{1}{\beta} \log(1 + \exp(\beta \mathbf{x})),$$

with $\beta = \log(2) \approx 0.693$ to output 1 for $\mathbf{x} = 0$.

Training took approximately two days on a single NVIDIA GTX 1080 Ti graphics card.

B.2. BIVA

For the BIVA model (Maaløe et al., 2019), we use a specification that is very similar to that of the HVAE above, and to that of the original paper. The model has 3 spatial latent variables with the rest being densely connected in order to have an architecture similar to the HVAE. The model uses an overall stride of 8, achieved by striding by 2 in the first, fourth and sixth deterministic transformations.

Training took approximately a week on a single NVIDIA GTX 1080 Ti graphics card.

C. Analysis of the influence of latent variables on the marginal likelihood

In the paper, we argue that the lowest level latent variables, which have the highest dimensionality, contribute the most to the approximate likelihood. Here, we provide a stringent mathematical argument that generalizes this to the exact marginal likelihood in a model with a deterministic decoder.

Hyperparameter	Setting/Range
All	
Optimization	Adam (Kingma & Ba, 2014)
Learning rate	$3e - 4$
Batch size	128
Epochs	2000
Free bits	2 nats per \mathbf{z}
Free bits constant	200 epochs
Free bits annealed	200 epochs
Activation	ReLU
Initialization	Data-dependent (Salimans & Kingma, 2016)
HVAE	
Convolution kernel	5-3-3
Stride	2-2-2 (natural) / 2-2-1 (grey)
Warmup anneal period	200 epochs
BIVA	
Convolution kernel	5-3-3-3-3-3-3-3-3
Stride	2-1-1-2-1-2-1-1-1-1

Table 4. Selection of most important hyperparameters and their setting. See Appendix B for more details.

C.1. Model specification

For an arbitrary hierarchical latent variable model, we have a prior $p(\mathbf{z}_L)$ and a generative mapping $f : \mathbb{R}^d \rightarrow \mathbb{R}^D$, such that $\mathbf{x} = f(\mathbf{z}_L)$ and $D > d$. Note that we will assume that f is deterministic, such that we are effectively working with $p(\mathbf{x}|\mathbf{z}) = \delta_{f(\mathbf{z})}(\mathbf{x})$. This is a limiting assumption, but it allows working through the following. For shorthand we will simply write $\mathbf{z} = \mathbf{z}_L$.

Let f have a bottleneck architecture, i.e.

$$f(\mathbf{z}) = f_1(\dots f_{L-1}(f_L(\mathbf{z}))), \quad (11)$$

where

$$f_i : \mathbb{R}^{d_i} \rightarrow \mathbb{R}^{d_{i-1}}, \quad i = L, \dots, 1. \quad (12)$$

Here we use the notation $d_0 = D = |\mathbf{x}|$ and $d_L = d = |\mathbf{z}|$ and further assume $d_0 \geq d_1 \geq \dots \geq d_{L-1} \geq d_L$ which gives the bottleneck.

Assuming \mathbf{x} is such that a corresponding latent variable \mathbf{z} exists, i.e. that there exists \mathbf{z} such that $\mathbf{x} = f(\mathbf{z})$, then we can write the likelihood of \mathbf{x} through a standard change of variables (similar to flow-based models),

$$p(\mathbf{x}) = p(\mathbf{z}) \prod_{i=1}^L \left(\sqrt{\det \mathbf{J}_i^T \mathbf{J}_i} \right)^{-1}, \quad (13)$$

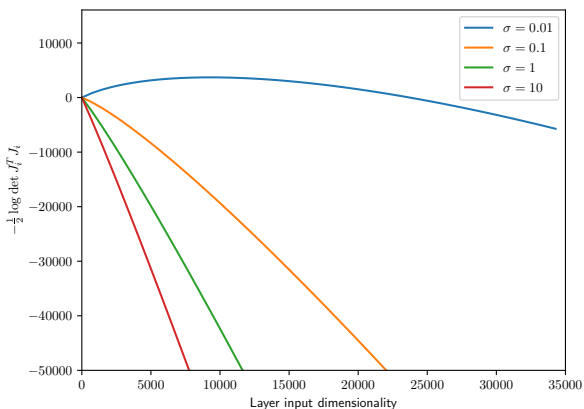


Figure 8. The expected inverse volume change for Gaussian Jacobians (17) on a log-scale.

where \mathbf{J}_i is the Jacobian of f_i , i.e.

$$\mathbf{J}_i = \frac{\partial f_i}{\partial \mathbf{z}_i} \in \mathbb{R}^{d_i \times d_{i-1}}. \quad (14)$$

Here we use the notation that \mathbf{z}_i is the representation at layer i . Note that $\mathbf{J}_i^T \mathbf{J}_i$ is a $d_{i-1} \times d_{i-1}$ symmetric positive semidefinite matrix (determinant ≥ 0).

The log-likelihood can be written as

$$\log p(\mathbf{x}) = \log p(\mathbf{z}) - \frac{1}{2} \sum_{i=1}^L \log \det \mathbf{J}_i^T \mathbf{J}_i. \quad (15)$$

By construction of determinants, we can generally expect these determinants to grow with the dimensionality of the matrix. We should expect the determinant of a $d \times d$ matrix to be of the order $\mathcal{O}(\lambda^d)$ for some number $\lambda > 0$. With that in mind, we should generally expect that

$$\det \mathbf{J}_{i+1}^T \mathbf{J}_{i+1} > \det \mathbf{J}_i^T \mathbf{J}_i, \quad (16)$$

due to the bottleneck assumption. If so, we see that the marginal likelihood $p(\mathbf{x})$ will be dominated by $\left(\sqrt{\det \mathbf{J}_1^T \mathbf{J}_1} \right)^{-1}$, i.e. low-level features have a higher influence on the likelihood than more important semantic ones.

C.2. The Gaussian case

The previous remarks can be made more precise if we make distributional assumptions on the Jacobians. Here we will assume that the Jacobians of each layer follow a Gaussian distribution. Specifically, we will assume that each entry in \mathbf{J}_i is distributed as $\mathcal{N}(0, \sigma^2)$. The analysis below extends to nonzero means and more general covariance structure, but this comes with a cost of less transparent notation. In this

setting, $\mathbf{J}_i^T \mathbf{J}_i$ follows a Wishart distribution (in the general setting it would follow a non-central Wishart distribution). Muirhead (2009) tells us that the expected multiplicative contribution to the likelihood of each layer is

$$\begin{aligned} \mathbb{E} \left[\left(\sqrt{\det \mathbf{J}_i^T \mathbf{J}_i} \right)^{-1} \right] &= \sigma^{-d_{i-1}} 2^{-\frac{d_{i-1}}{2}} \frac{\Gamma_{d_{i-1}} \left(\frac{1}{2} d_i - \frac{1}{2} \right)}{\Gamma_{d_{i-1}} \left(\frac{1}{2} d_i \right)} \\ &= \sigma^{-d_{i-1}} 2^{-\frac{d_{i-1}}{2}} \frac{\Gamma \left(\frac{1}{2} (d_i - d_{i-1}) \right)}{\Gamma \left(\frac{1}{2} d_i \right)} \end{aligned} \quad (17)$$

where Γ_d is the multivariate Gamma function. Assuming that the increase in layer dimension $d_i - d_{i-1}$ is constant, then we see that (17) goes to zero as d_i goes to infinity as the Γ function grows super-exponentially to infinity. This super-exponential growth further implies that the first layers dominate the marginal likelihood $p(\mathbf{x})$. This is also visually evident in Figure 8.

D. Derivation of the $\mathcal{L}^{>k}$ bound

In this section we present the derivation of $\mathcal{L}^{>k}$ and show that it is a lower bound on the marginal likelihood.

First, we consider a two-layered VAE with bottom-up inference. We proceed very similarly to the derivation of the regular ELBO and also use Jensen's inequality.

$$\begin{aligned} \log p(\mathbf{x}) &= \log \int \int p(\mathbf{x}|\mathbf{z}_1) p(\mathbf{z}_1|\mathbf{z}_2) p(\mathbf{z}_2) d\mathbf{z}_1 d\mathbf{z}_2 \quad (18) \\ &= \log \int \int \frac{q(\mathbf{z}_2|\mathbf{x})}{q(\mathbf{z}_2|\mathbf{x})} p(\mathbf{x}|\mathbf{z}_1) p(\mathbf{z}_1|\mathbf{z}_2) p(\mathbf{z}_2) d\mathbf{z}_1 d\mathbf{z}_2 \\ &= \log \int \int q(\mathbf{z}_2|\mathbf{x}) p(\mathbf{z}_1|\mathbf{z}_2) \frac{p(\mathbf{x}|\mathbf{z}_1) p(\mathbf{z}_2)}{q(\mathbf{z}_2|\mathbf{x})} d\mathbf{z}_1 d\mathbf{z}_2 \\ &\geq \mathbb{E}_{p(\mathbf{z}_1|\mathbf{z}_2) q(\mathbf{z}_2|\mathbf{x})} \left[\log \frac{p(\mathbf{x}|\mathbf{z}_1) p(\mathbf{z}_2)}{q(\mathbf{z}_2|\mathbf{x})} \right] \equiv \mathcal{L}^{>1} . \end{aligned}$$

Here, we have introduced the variational distribution $q(\mathbf{z}_2|\mathbf{x})$ which, naively, is different from any of the available variational distributions $q(\mathbf{z}_1|\mathbf{x})$ and $q(\mathbf{z}_2|\mathbf{z}_1)$. However, it's easy to see that we can simply define $q(\mathbf{z}_2|\mathbf{x}) = q(\mathbf{z}_2|d_1(\mathbf{x}))$ where $d_1(\mathbf{x}) = \mathbb{E}[q(\mathbf{z}_1|\mathbf{x})]$. I.e. we compute the distribution over \mathbf{z}_2 via the mode of $q(\mathbf{z}_1|\mathbf{x})$. This is possible since we exclusively manipulate the variational proposal distribution without altering the generative model $p(\mathbf{x}, \mathbf{z})$.

In general, the derivation of $\mathcal{L}^{>k}$ for an L -layered hierarchi-

cal VAE with $\mathbf{z} = \mathbf{z}_1, \dots, \mathbf{z}_L$ is as follows:

$$\begin{aligned} \log p(\mathbf{x}) &= \log \int p(\mathbf{x}|\mathbf{z}) p(\mathbf{z}) d\mathbf{z} \quad (19) \\ &= \log \int \frac{q(\mathbf{z}_{>k}|\mathbf{x})}{q(\mathbf{z}_{>k}|\mathbf{x})} p(\mathbf{x}|\mathbf{z}) p(\mathbf{z}) d\mathbf{z} \\ &= \log \int q(\mathbf{z}_{>k}|\mathbf{x}) p(\mathbf{z}) \frac{p(\mathbf{x}|\mathbf{z})}{q(\mathbf{z}_{>k}|\mathbf{x})} d\mathbf{z} \\ &= \log \int q(\mathbf{z}_{>k}|\mathbf{x}) p(\mathbf{z}_{\leq k}|\mathbf{z}_{>k}) p(\mathbf{z}_{>k}) \frac{p(\mathbf{x}|\mathbf{z})}{q(\mathbf{z}_{>k}|\mathbf{x})} d\mathbf{z} \\ &= \log \int q(\mathbf{z}_{>k}|\mathbf{x}) p(\mathbf{z}_{\leq k}|\mathbf{z}_{>k}) \frac{p(\mathbf{x}|\mathbf{z}) p(\mathbf{z}_{>k})}{q(\mathbf{z}_{>k}|\mathbf{x})} d\mathbf{z} \\ &\geq \mathbb{E}_{p(\mathbf{z}_{\leq k}|\mathbf{z}_{>k})} \left[\log q(\mathbf{z}_{>k}|\mathbf{x}) \frac{p(\mathbf{x}|\mathbf{z}) p(\mathbf{z}_{>k})}{q(\mathbf{z}_{>k}|\mathbf{x})} \right] \\ &\geq \mathbb{E}_{p(\mathbf{z}_{\leq k}|\mathbf{z}_{>k}) q(\mathbf{z}_{>k}|\mathbf{x})} \left[\log \frac{p(\mathbf{x}|\mathbf{z}) p(\mathbf{z}_{>k})}{q(\mathbf{z}_{>k}|\mathbf{x})} \right] \equiv \mathcal{L}^{>k} . \end{aligned}$$

Similar to the $L = 2$ case above, we have defined

$$q(\mathbf{z}_{>k}|\mathbf{x}) = q(\mathbf{z}_{>k}|d_k(\mathbf{x}))$$

with d_k defined recursively as

$$d_k(\mathbf{x}) = \mathbb{E}[q(\mathbf{z}_k|d_{k-1}(\mathbf{x}))], \quad d_0(\mathbf{x}) = \mathbf{x} .$$

That is, we simply consider the inference network below \mathbf{z}_{k+1} to be a deterministic encoder and forward pass the mode of each preceding variational distribution.

Additionally, we obtain $p(\mathbf{z}_{\leq k}|\mathbf{z}_{>k}) p(\mathbf{z}_{>k})$ by splitting

$$p(\mathbf{z}) = p(\mathbf{z}_L) p(\mathbf{z}_{L-1}|\mathbf{z}_L) \cdots p(\mathbf{z}_1|\mathbf{z}_2)$$

at index k . Importantly, we then evaluate

$$p(\mathbf{z}_{>k}) = p(\mathbf{z}_L) p(\mathbf{z}_{L-1}|\mathbf{z}_L) \cdots p(\mathbf{z}_{k+1}|\mathbf{z}_{k+2})$$

with samples from $q(\mathbf{z}_{>k}|\mathbf{x})$ while

$$p(\mathbf{z}_{\leq k}|\mathbf{z}_{>k}) = p(\mathbf{z}_k|\mathbf{z}_{k+1}) p(\mathbf{z}_{k-1}|\mathbf{z}_k) \cdots p(\mathbf{z}_1|\mathbf{z}_2)$$

is evaluated for \mathbf{z}_k with $\mathbf{z}_{k+1} \sim q(\mathbf{z}_{>k}|\mathbf{x})$ and for $\mathbf{z}_{<k}$ with $\mathbf{z}_{>k}$ obtained conditionally from itself.

E. The complementary $\mathcal{L}^{<l}$ bound

We can generalize the $\mathcal{L}^{>k}$ bound by introducing the flipped version, $\mathcal{L}^{<l}$, which compared to $\mathcal{L}^{>k}$, instead samples the $L - l$ highest latent variables in the hierarchy from the prior $\mathbf{z}_1, \dots, \mathbf{z}_L \sim p_\theta(\mathbf{z}_{\geq l}) = p_\theta(\mathbf{z}_l|\mathbf{z}_{l+1}) \cdots p_\theta(\mathbf{z}_L)$ and the remaining lower latents from the approximate posterior $\hat{\mathbf{z}}_1, \dots, \hat{\mathbf{z}}_{l-1} \sim q_\phi(\mathbf{z}_{<l}|\mathbf{x}) = q_\phi(\mathbf{z}_1|\mathbf{x}) q_\phi(\mathbf{z}_2|\mathbf{z}_1) \cdots q_\phi(\mathbf{z}_{l-1}|\mathbf{z}_{l-2})$,

$$\mathcal{L}^{<l} = \mathbb{E}_{p_\theta(\mathbf{z}_{\geq l}) q_\phi(\mathbf{z}_{<l}|\mathbf{x})} \left[\log \frac{p_\theta(\mathbf{x}, \mathbf{z}) p_\theta(\mathbf{z}_{<l})}{q_\phi(\mathbf{z}_{<l}|\mathbf{x})} \right] . \quad (20)$$

Similar to $\mathcal{L}^{>k}$, we recover the regular ELBO for $l = L$. Contrary to $\mathcal{L}^{>k}$, this bound puts as much emphasis on the lowest latent variables as the regular ELBO but keeps track of large deviation from the unconditional prior in the top $L - l$ KL-terms since it is not guided by the approximate posterior for $\mathbf{z}_{>l}$.

While this bound is not expected to improve OOD detection by itself, mainly since the data likelihood $p(\mathbf{x}|\mathbf{z})$ is the same as for the ELBO, we can incorporate it in a generalized log likelihood-ratio between $\mathcal{L}^{<l}$ and $\mathcal{L}^{>k}$

$$LLR_{<l}^{>k} = \mathcal{L}^{<l} - \mathcal{L}^{>k}. \quad (21)$$

We conjecture that this score, or the other possible permutations of it, might be useful for OOD detection but leave further examination to future work.

F. Note on the KL-term of hierarchical VAEs

In this research we choose model parameterizations relying on bottom-up inference (Burda et al., 2016),

$$q_\phi(\mathbf{z}|\mathbf{x}) = q_\phi(\mathbf{z}_1|\mathbf{x}) \prod_{i=2}^L q_\phi(\mathbf{z}_i|\mathbf{z}_{i-1}). \quad (22)$$

We do this because bottom-up inference enables the model to learn covariance between the latent variables in the hierarchy. In the inference model, any latent variable is dependent on the latent variables below it in the hierarchy and, importantly, the top most latent variable is dependent on all other latent variables.

In contrast, a top-down inference model (Sønderby et al., 2016) has a topmost latent variable \mathbf{z}_L that is independent of the other latent variables and is directly given by \mathbf{x} .

$$q_\phi(\mathbf{z}|\mathbf{x}) = q_\phi(\mathbf{z}_L|\mathbf{x}) \prod_{i=L-1}^1 q_\phi(\mathbf{z}_i|\mathbf{z}_{i+1}). \quad (23)$$

This, in essence, makes \mathbf{z}_L a mean-field approximation without any covariance structure tying it to the other latent variables, $\text{Cov}(z_{L,i}, z_{k,j}) = 0$ for $k < L$. Furthermore, since the approximate posterior (and the prior) typically have diagonal covariance, \mathbf{z}_L is also mean-field within its own elements, $\text{Cov}(z_{L,i}, z_{L,j}) = 0$ for $i \neq j$.

We hypothesize that the covariance of latent variables towards the top of the hierarchy with other latent variables is important for learning semantic representations. However, top-down inference models are easier to optimize as has recently been demonstrated (Sønderby et al., 2016; Vahdat & Kautz, 2020; Child, 2021).

In the following, we inspect the differences between the ELBO used for bottom-up inference and the ELBO used for top-down inference and show that it is not generally possible to decompose the total KL-divergence into separate KL-divergences per latent variable. Specifically, for top-down inference it is possible to obtain KL-divergence at

the top-most latent variable and an expectation of a KL-divergence for the other latent variables. For bottom-up inference, the resulting terms are no longer KL-divergences except at the top-most latent variable.

We ask the question whether models relying on top-down inference are impeded in their use for semantic OOD detection, or whether they still learn to assign a more semantic representation in the top-most variables simply due to the flexibility of the deterministic neural network layers. This remains an open research question.

F.1. Bottom-up inference

By splitting up the expectation, we can write the ELBO of a two-layer bottom-up hierarchical VAE as

$$\begin{aligned} \log p(\mathbf{x}) &\geq \mathbb{E}_{q(\mathbf{z}_1, \mathbf{z}_2|\mathbf{x})} [\log p(\mathbf{x}|\mathbf{z}_1)] & (24) \\ &+ \mathbb{E}_{q(\mathbf{z}_1, \mathbf{z}_2|\mathbf{x})} [\log p(\mathbf{z}_1|\mathbf{z}_2) - \log q(\mathbf{z}_1|\mathbf{x})] \\ &+ \mathbb{E}_{q(\mathbf{z}_1, \mathbf{z}_2|\mathbf{x})} [\log p(\mathbf{z}_2) - \log q(\mathbf{z}_2|\mathbf{z}_1)]. \end{aligned}$$

We can write out the expectations in order to derive the KL-divergence terms of the bottom-up ELBO:

$$\begin{aligned} \log p(\mathbf{x}) &\geq \int \int \log p(\mathbf{x}|\mathbf{z}_1) d\mathbf{z}_2 d\mathbf{z}_1 & (25) \\ &+ \int q(\mathbf{z}_1|\mathbf{x}) \int q(\mathbf{z}_2|\mathbf{z}_1) \log \frac{p(\mathbf{z}_1|\mathbf{z}_2)}{q(\mathbf{z}_1|\mathbf{x})} d\mathbf{z}_2 d\mathbf{z}_1 \\ &+ \int q(\mathbf{z}_1|\mathbf{x}) \int q(\mathbf{z}_2|\mathbf{z}_1) \log \frac{p(\mathbf{z}_2)}{q(\mathbf{z}_2|\mathbf{z}_1)} d\mathbf{z}_2 d\mathbf{z}_1. \end{aligned}$$

From the above, we can see that since the decomposition is in a reverse order, we cannot derive the KL-divergence for the second term. This will hold in general for L -layered models for any latent variables $\mathbf{z}_1, \dots, \mathbf{z}_{L-1}$:

$$\begin{aligned} \log p(\mathbf{x}) &\geq \mathbb{E}_{q(\mathbf{z}_1, \mathbf{z}_2|\mathbf{x})} [\log p(\mathbf{x}|\mathbf{z}_1)] & (26) \\ &+ \mathbb{E}_{q(\mathbf{z}_1|\mathbf{x})} \left[\mathbb{E}_{q(\mathbf{z}_2|\mathbf{z}_1)} \left[\log \frac{p(\mathbf{z}_1|\mathbf{z}_2)}{q(\mathbf{z}_1|\mathbf{x})} \right] \right] \\ &+ \mathbb{E}_{q(\mathbf{z}_1|\mathbf{x})} [-D_{\text{KL}}[q(\mathbf{z}_2|\mathbf{z}_1)||p(\mathbf{z}_2)]] . \end{aligned}$$

F.2. Top-down inference

By splitting up the expectation, we can write the ELBO of a two-layer top-down hierarchical VAE as

$$\begin{aligned} \log p(\mathbf{x}) &\geq \mathbb{E}_{q(\mathbf{z}_1, \mathbf{z}_2|\mathbf{x})} [\log p(\mathbf{x}|\mathbf{z}_1)] & (27) \\ &+ \mathbb{E}_{q(\mathbf{z}_1, \mathbf{z}_2|\mathbf{x})} [\log p(\mathbf{z}_2|\mathbf{x}) - \log q(\mathbf{z}_2|\mathbf{x})] \\ &+ \mathbb{E}_{q(\mathbf{z}_1, \mathbf{z}_2|\mathbf{x})} [\log p(\mathbf{z}_1|\mathbf{z}_2) - \log q(\mathbf{z}_1|\mathbf{z}_2)]. \end{aligned}$$

OOD dataset	Metric	AUROC \uparrow	AUPRC \uparrow	FPR80 \downarrow
Trained on SVHN				
CIFAR10	$L^{>0}$	0.992	0.993	0.004
CIFAR10	$L^{>1}$	0.988	0.990	0.002
CIFAR10	$L^{>2}$	0.746	0.756	0.468
CIFAR10	$LLR^{>1}$	0.939	0.950	0.052
SVHN	$L^{>0}$	0.599	0.587	0.702
SVHN	$L^{>1}$	0.555	0.543	0.755
SVHN	$L^{>2}$	0.403	0.431	0.869
SVHN	$LLR^{>1}$	0.489	0.484	0.799

Table 5. Additional results for the HVAE model trained on SVHN. All results computed with 1000 importance samples.

We can write out the expectations in order to derive the KL-divergence terms:

$$\begin{aligned} \log p(\mathbf{x}) &\geq \int \int \log p(\mathbf{x}|\mathbf{z}_1) d\mathbf{z}_1 \mathbf{z}_2 & (28) \\ &+ \int q(\mathbf{z}_2|\mathbf{x}) \log \frac{p(\mathbf{z}_2|\mathbf{x})}{q(\mathbf{z}_2|\mathbf{x})} d\mathbf{z}_2 \\ &+ \int q(\mathbf{z}_2|\mathbf{x}) \int q(\mathbf{z}_1|\mathbf{z}_2) \log \frac{p(\mathbf{z}_1|\mathbf{z}_2)}{q(\mathbf{z}_1|\mathbf{z}_2)} d\mathbf{z}_1 \mathbf{z}_2 . \end{aligned}$$

The KL-divergence terms can now easily be computed by:

$$\begin{aligned} \log p(\mathbf{x}) &\geq \mathbb{E}_{q(\mathbf{z}_1, \mathbf{z}_2|\mathbf{x})} [\log p(\mathbf{x}|\mathbf{z}_1)] & (29) \\ &- D_{\text{KL}}[q(\mathbf{z}_2|\mathbf{x})||p(\mathbf{z}_2)] \\ &- \mathbb{E}_{q(\mathbf{z}_2|\mathbf{x})} [D_{\text{KL}}[q(\mathbf{z}_1|\mathbf{z}_2)||p(\mathbf{z}_1|\mathbf{z}_2)] . \end{aligned}$$

Note that the KL-divergence in the second layer is not exact since it is dependent on the sample-noise from the layer below. An exact solution can only be derived if the latent variables \mathbf{z} are all conditionally independent. However, this comes at the cost of not learning a covariance structure.

G. Additional results

We provide additional results for a model trained on FashionMNIST in Table 7, a model trained on MNIST in Table 8, a model trained on CIFAR10 in Table 6 and a model trained on SVHN in Table 5.

We note that while the likelihood is highly unreliable across the datasets, the proposed log likelihood-ratio score is consistent and always allows correct OOD detection with high AUROC \uparrow .

OOD dataset	Metric	AUROC \uparrow	AUPRC \uparrow	FPR80 \downarrow
Trained on CIFAR10				
SVHN	$L^{>0}$	0.083	0.318	0.974
SVHN	$L^{>1}$	0.097	0.320	0.972
SVHN	$L^{>2}$	0.693	0.725	0.599
SVHN	$LLR^{>2}$	0.811	0.837	0.394
CIFAR10	$L^{>0}$	0.485	0.488	0.817
CIFAR10	$L^{>1}$	0.467	0.476	0.822
CIFAR10	$L^{>2}$	0.411	0.433	0.869
CIFAR10	$LLR^{>1}$	0.469	0.479	0.835

Table 6. Additional results for the HVAE model trained on CIFAR10. All results computed with 1000 importance samples.

OOD dataset	Metric	AUROC \uparrow	AUPRC \uparrow	FPR80 \downarrow
Trained on FashionMNIST				
MNIST	$\mathcal{L}^{>0}$	0.268	0.363	0.882
MNIST	$\mathcal{L}^{>1}$	0.593	0.591	0.658
MNIST	$\mathcal{L}^{>2}$	0.712	0.750	0.548
MNIST	$LLR^{>1}$	0.986	0.987	0.011
notMNIST	$\mathcal{L}^{>0}$	0.916	0.932	0.116
notMNIST	$\mathcal{L}^{>1}$	0.983	0.986	0.000
notMNIST	$\mathcal{L}^{>2}$	0.997	0.997	0.000
notMNIST	$LLR^{>1}$	0.998	0.998	0.000
KMNIST	$\mathcal{L}^{>0}$	0.690	0.694	0.554
KMNIST	$\mathcal{L}^{>1}$	0.835	0.863	0.359
KMNIST	$\mathcal{L}^{>2}$	0.844	0.875	0.339
KMNIST	$LLR^{>1}$	0.974	0.977	0.017
Omniglot28x28	$\mathcal{L}^{>0}$	0.898	0.837	0.166
Omniglot28x28	$\mathcal{L}^{>1}$	0.991	0.989	0.011
Omniglot28x28	$\mathcal{L}^{>2}$	1.000	1.000	0.000
Omniglot28x28	$LLR^{>2}$	1.000	1.000	0.000
Omniglot28x28Inverted	$\mathcal{L}^{>0}$	0.261	0.361	0.879
Omniglot28x28Inverted	$\mathcal{L}^{>1}$	0.450	0.431	0.709
Omniglot28x28Inverted	$\mathcal{L}^{>2}$	0.557	0.574	0.678
Omniglot28x28Inverted	$LLR^{>1}$	0.954	0.954	0.050
SmallNORB28x28	$\mathcal{L}^{>0}$	0.982	0.984	0.000
SmallNORB28x28	$\mathcal{L}^{>1}$	0.998	0.998	0.000
SmallNORB28x28	$\mathcal{L}^{>2}$	1.000	1.000	0.000
SmallNORB28x28	$LLR^{>2}$	0.999	0.999	0.002
SmallNORB28x28Inverted	$\mathcal{L}^{>0}$	0.965	0.971	0.000
SmallNORB28x28Inverted	$\mathcal{L}^{>1}$	0.997	0.992	0.000
SmallNORB28x28Inverted	$\mathcal{L}^{>2}$	0.981	0.985	0.000
SmallNORB28x28Inverted	$LLR^{>2}$	0.941	0.946	0.069
FashionMNIST	$\mathcal{L}^{>0}$	0.476	0.484	0.816
FashionMNIST	$\mathcal{L}^{>1}$	0.475	0.482	0.817
FashionMNIST	$\mathcal{L}^{>2}$	0.475	0.484	0.823
FashionMNIST	$LLR^{>1}$	0.488	0.496	0.811

Table 7. Additional results for the HVAE model trained on FashionMNIST. All results computed with 1000 importance samples.

OOD dataset	Metric	AUROC \uparrow	AUPRC \uparrow	FPR80 \downarrow
Trained on MNIST				
FashionMNIST	$L^{>0}$	1.000	1.000	0.000
FashionMNIST	$L^{>1}$	1.000	1.000	0.000
FashionMNIST	$L^{>2}$	0.981	0.983	0.003
FashionMNIST	$LLR^{>1}$	0.999	0.999	0.000
notMNIST	$L^{>0}$	1.000	1.000	0.000
notMNIST	$L^{>1}$	1.000	1.000	0.000
notMNIST	$L^{>2}$	1.000	1.000	0.000
notMNIST	$LLR^{>1}$	1.000	0.999	0.000
KMNIST	$L^{>0}$	1.000	1.000	0.000
KMNIST	$L^{>1}$	1.000	1.000	0.000
KMNIST	$L^{>2}$	0.987	0.987	0.011
KMNIST	$LLR^{>1}$	0.999	0.999	0.000
Omniglot28x28	$L^{>0}$	1.000	1.000	0.000
Omniglot28x28	$L^{>1}$	1.000	1.000	0.000
Omniglot28x28	$L^{>2}$	1.000	1.000	0.000
Omniglot28x28	$LLR^{>1}$	1.000	1.000	0.000
Omniglot28x28Inverted	$L^{>0}$	0.862	0.902	0.205
Omniglot28x28Inverted	$L^{>1}$	0.923	0.943	0.056
Omniglot28x28Inverted	$L^{>2}$	0.749	0.691	0.411
Omniglot28x28Inverted	$LLR^{>1}$	0.944	0.953	0.057
SmallNORB28x28	$L^{>0}$	1.000	1.000	0.000
SmallNORB28x28	$L^{>1}$	1.000	1.000	0.000
SmallNORB28x28	$L^{>2}$	1.000	1.000	0.000
SmallNORB28x28	$LLR^{>1}$	1.000	1.000	0.000
SmallNORB28x28Inverted	$L^{>0}$	1.000	1.000	0.000
SmallNORB28x28Inverted	$L^{>1}$	1.000	1.000	0.000
SmallNORB28x28Inverted	$L^{>2}$	0.977	0.980	0.001
SmallNORB28x28Inverted	$LLR^{>1}$	0.985	0.987	0.000
MNIST	$L^{>0}$	0.488	0.486	0.807
MNIST	$L^{>1}$	0.469	0.469	0.816
MNIST	$L^{>2}$	0.514	0.505	0.791
MNIST	$LLR^{>2}$	0.515	0.507	0.792

Table 8. Additional results for the HVAE model trained on MNIST. All results computed with 1000 importance samples.